Journal of
Materials Chemistry A

Accepted Manuscript

This is an *Accepted Manuscript*, which has been through the RSC Publishing peer review process and has been accepted for publication.

Accepted Manuscripts are published online shortly after acceptance, which is prior to technical editing, formatting and proof reading. This free service from RSC Publishing allows authors to make their results available to the community, in citable form, before publication of the edited article. This *Accepted Manuscript* will be replaced by the edited and formatted *Advance Article* as soon as this is available.

To cite this manuscript please use its permanent Digital Object Identifier (DOI®), which is identical for all formats of publication.

More information about *Accepted Manuscripts* can be found in the **Information for Authors**.

Please note that technical editing may introduce minor changes to the text and/or graphics contained in the manuscript submitted by the author(s) which may alter content, and that the standard **Terms & Conditions** and the **ethical guidelines** that apply to the journal are still applicable. In no event shall the RSC be held responsible for any errors or omissions in these *Accepted Manuscript* manuscripts or any consequences arising from the use of any information contained in them.

Superior Dye Adsorption Capacity of Amorphous WO_3 Sub-micrometer Rods Fabricated by Glancing Angle Deposition†

Pradip Basnet,[a]* and Yiping Zhao[a]

[a] *Department of Physics and Astronomy, and Nanoscale Science and Engineering Center, University of Georgia, Athens, Georgia 30602*

Corresponding author. E-mail: pbasnet@physast.uga.edu. Phone: +1-706-542-6230. Fax: +1-706-542-2492.

Porous, amorphous tungsten trioxide (WO_3) sub micrometer rods (SMRs), fabricated by glancing angle deposition technique, were observed to exhibit superior methylene blue (MB) adsorption capability in aqueous solution due to their large specific surface area and active surface functionality. The adsorption of MB on the surface of WO_3 SMRs is well-described by Langmuir isotherm behavior.

The removal of reactive dye(s) from wastewater has attracted a lot of attention because most of the dyes are non-biodegradable, significantly toxic, and some of them are also carcinogenic.[1-5] Adsorption has been found to be one of the most efficient ways to remove the dye effluents from the environment.[4-6] The use of Silica, Zeolites, Peat, and Chitin as adsorbents is limited as they cannot meet the growing industrial demand due to limited adsorption capacity.[4, 7-10] Powdered or granular activated carbon has been considered as the excellent adsorbent materials.[6, 11-13] Nevertheless, carbon-based materials must be treated as hazardous waste when thorough removal is required for trace amount of toxic dye effluents.[14] It is clear that the ideal material for the removal of toxic dye effluents should offer both excellent adsorption capability and surface activity that can degrade harmful pollutants.

Nanostructured semiconductor photocatalysts not only can have high dye adsorption capability, but can also generate electron-hole pairs upon photon absorption. They can degrade toxic pollutants into harmless by-products through photocatalytic reactions. In particular, tungsten trioxide (WO_3) has recently emerged as an excellent photocatalytic material for dye removal.[15-17] However, their adsorption capability varies a

lot depending on the morphology and preparation techniques, as summarized in Table 1. Compared to good carbon materials, the adsorption capability of WO_3 is still low.

In this communication, we report that amorphous WO_3 sub micrometer rods (SMRs) fabricated by glancing angle deposition has superior cationic dye adsorption capability that is comparable to that of the granular activated carbon.

We used the glancing angle deposition (GLAD) technique to fabricate amorphous WO_3 nanorod arrays onto glass and silicon substrates. GLAD is a well-known physical vapor deposition technique that can create porous thin films composed of arrays of fibrous nanorods.[18-21] The experimental details for the amorphous WO_3 SMR preparation and annealing are provided in Part I and Part VII of the of the ESI†. As shown by the scanning electron micrographs (SEM; FEI Inspect F) (Fig. 1a & 1b) and transmission electron microscope (TEM; FEI Tecnai 20) (Fig. 1c) images, the as-deposited WO_3 films consist of an array of well-aligned and fibrous SMRs. From the SEM images, the SMRs are found to have an average length, L = 1130 ± 30 nm, average diameter at top, d = 180 ± 40 nm, average SMRs separation, S = 130 ± 40 nm, and average SMRs density, η = 12 ± 3 μm^{-2}. These as-deposited amorphous WO_3 SMRs array samples were characterized structurally and optically (see Part II in ESI† for X-ray Diffraction (XRD) and UV-Vis results). The average Zeta-potential (Malvern Zetasizer Nano ZS, Model: ZN3600) of as-deposited WO_3 SMRs suspensions in pure DI water (18 MΩ·cm) were measured to be -39 mV at pH 8.1, indicating that the as-deposited WO_3 SMRs have an overall negative surface charge at slightly basic condition.

MB adsorption characterizations of the WO_3 SMRs samples in aqueous solution were performed at room temperature (25 ± 1 °C) with different initial MB concentrations

C_0 (from 50 to 100 μM) (see Part III in ESI† for details). Upon immersion of WO_3 SMRs sample into MB aqueous solution, the blue color of the MB aqueous solution was observed to disappear rapidly, which is attributed to fast MB adsorption onto the WO_3 surface. The mechanism of MB removal, by adsorption on WO_3 nanostructure, can be due to cationic form (MB^+) and the negative charged surface of WO_3 SMRs. And the overall adsorption can be assumed to involve the following steps: [6] migration of dye from bulk solution to the surface of the adsorbent, adsorption of dye at an active site on the surface of WO_3, and intra-particle diffusion of dye into the interior pores of the WO_3 nanostructure. In addition, the dye removal rate was observed to be enhanced noticeably with the UV light irradiation (λ = 365 nm), especially after 30 min, which is due to the slower photocatalytic degradation mechanism (see Part IV in ESI† for Fourier transform infrared (FT-IR) and UV-visible absorbance spectra confirming adsorbance on the surface and photocatalytic degradation under UV irradiation). For dark experiments, decoloration of MB solutions was observed to cease after a certain period, about 30 min for C_0 = 50 μM and 60 min for C_0 = 100 μM. We regarded this time as equilibrium adsorption-time; and it varied with C_0. For different C_0, the equilibrium adsorption capabilities q_e were estimated from the equilibrium MB concentration C_e, by using the mass balance relationship,

$$q_e(mol/g) = \frac{(C_0 - C_e)(mol/L)V(L)}{m(g)}, \quad (1)$$

where m and V are the mass of adsorbent and volume of the MB solution, respectively. The C_e was estimated spectrophotometrically using a calibration curve (see Part V in ESI†) and was examined for two different experimental conditions. One experiment measured the absorbance spectra for C_e of aliquot samples, where 2 mL volumes of

mixture solutions of MB with WO_3 SMRs were pipetted out at predetermined times after shaking in an orbital-shaker without centrifugation (WOC). And in the other experiment, the aliquot samples were collected with centrifugation (WC) at 15,000 rpm for 1 min followed by the absorbance spectra measurement for C_e (see Part III in ESI† for further experimental details). In both cases, q_e were observed to increase with increasing C_0 while the percentage removals of MB concentrations $[(C_0 - C_e)/C_0 \times 100]$ were observed to decrease. It is worthwhile to mention that for the WOC process, 92.6 % removal of MB concentrations were observed for C_0 = 50 μM in 30 mins, while 74.6 % removal for C_0 = 100 μM in 60 mins. The WC process was observed to cause a further enhancement in adsorption capability. For the two concentrations above, the percentage removals were increased to 94.4 and 78.4 % respectively. The adsorption isotherms for both the WC and WOC processes were obtained after the adsorption for 90 min, and C_e/q_e *versus* C_e is plotted in Fig. 2. Both plots seem to follow a linear relationship, which indicates a Langmuir isotherm process, for which

$$\frac{C_e}{q_e} = \frac{1}{Q_m K} + \left(\frac{1}{Q_m}\right) C_e, \qquad (2)$$

where Q_m and K are the Langmuir constants related to monolayer adsorption capacity (mol/g) and surface energy (L/mol) at equilibrium, respectively.[6, 22-24] Both the Q_m and K values can be obtained from linear fitting: for WOC process, Q_m = 750 ± 20 μmol/g, K = 0.21 L/μmol and for WC process, Q_m = 780 ± 20 μmol/g, K = 0.32 L/μmol. The equivalent Q_m values are estimated to be 240 and 250 mg/g respectively for WOC and WC. These Q_m values are 30 ~ 31 times higher than those reported for crystalline WO_3 nanoparticles synthesized by combustion method[15] and comparable to granular activated carbon.[17] To the best of our knowledge, these amorphous WO_3 SMRs exhibited the best

adsorption capacity among any other WO_3 nanostructures, fabricated by different methods.[15, 25, 26] Not surprisingly, we obtained a higher Q_m value for the WC experiment since the centrifugation can allow the MB molecules to access more WO_3 surfaces, such as nanopores or nano-fibrous surfaces. In addition, we observed that WC process break the WO_3 SMRs into sponge-like nanoscale networks which further confirms the increase of surface area (see Part VI in ESI†, for SEM and TEM images for change in morphology). Such a network structure is the result of high mechanical force applied to the sample during centrifugation. However, if the amorphous WO_3 SMRs were annealed to change their crystalline phase, the dye adsorption properties will also change. MB adsorption experiments have been performed on the WO_3 samples annealed at T = 300, 400, 500 and 550 °C, respectively (see Part VII in ESI†). With increased annealing temperature, the MB adsorption decreases. This could be primarily due to the decrease in total surface area of the nanostructure *via* crystallization and coarsening of nanorods.

Similar adsorption experiments have been performed on three other dyes for amorphous WO_3 SMRs, one cationic dye Rhodamine 6G (R6G), and two anionic dyes, Methylene Orange (MO) and Phenol (Ph) under similar experimental conditions (see Part VIII in ESI†, for other dye adsorption experiments). The adsorption capacity of R6G is similar to that of MB, while for MO and Ph little adsorption has been observed (see Table S1 in Part VIII of ESI†). This suggests that the dye adsorption process onto WO_3 nanoorod surface is dominated by the electrostatic interaction.

Besides the adsorption capacities, the kinetics of dye removal is also investigated through the time-dependent MB concentration measurement during adsorption. A typical plot of remaining MB concentration in solution, $C(t)$, for C_0 = 50 μM versus adsorption

time t is shown in Fig. 3a for both WC and WOC processes. The inset photographs show the color change of the solution before and after reaching adsorption equilibrium (t = 30 min). The rapid MB adsorption at the initial stage (~10 mins for 50 μM) may be attributed to stronger electrostatic attraction and also the more available surface area. This tendency becomes slower as the time passes due to the less vacant adsorption sites available for MB molecules (until the adsorption saturation is attained). From $C(t)$, the time dependent quantity of adsorbed MB, q_t was calculated using Eq. (1). Since the adsorption follows the Langmuir isotherm, the $q_t \sim t$ relation should be determined by a pseudo-second-order kinetic model,[23, 27, 28]

$$\frac{dq_t}{dt} = K_2 (q_e - q_t)^2, \tag{3}$$

where K_2 is the rate constant of pseudo-second-order model. Eq. (3) can be reduced to

$$\frac{t}{q_t} = \frac{1}{K_2 q_e^{\,2}} + \frac{t}{q_e}. \tag{4}$$

The plot of t/q_t versus t should show a linear relation, and the data fitting can extract K_2 and $1/K_2 q_e^2$. The plots of t/q_t versus t, including fitting values of K_2, $K_2 q_e^2$, and fitting correlation coefficients, are presented in Part IX of ESI†. The results show that the K_2 is a complex function of C_0, as described by Azizian's theoretical analysis.[27] In fact, based on Azizian's paper, the adsorption rates K_a, as a function of C_0, can be estimated by

$$K_a = \frac{2 q_e K_2}{\left[\frac{(C_0 - C_e)}{\theta_e} + C_0 + \sqrt{\left[\frac{(C_0 - C_e)}{\theta_e} + C_0\right]^2 - 4 C_0 \frac{(C_0 - C_e)}{\theta_e}}\right]}, \tag{5}$$

and K_a can be used to describe the adsorption process. Fig. 3(b) shows that in general K_a decreases with C_0 monotonically (except the data point at C_0 = 60 μM). This result is

consistent with a report by Tsai *et. al*. for adsorption of acid dyes from aqueous solution on activated bleaching earth.[29] However, at higher concentrations, $C_0 \geq 80$ μM, the K_a values were observed to approach a constant. This could be attributed to the fact that the MB adsorptions at higher concentration will not follow the Langmuir type adsorption, and a pseudo-first-order reaction can be used to better describe the process.[27] In fact, for high MB concentration data ($C_0 \geq 80$ μM) the pseudo-first-order model gives better data fitting (see in Part IX of ESI† for pseudo-first-order model and Table S2 for fitting results).

In conclusion, we have demonstrated that the GLAD prepared amorphous WO_3 SMRs exhibit superior adsorption capability for MB. The adsorption kinetic studies show that the removal of MB from aqueous solution is a rapid process and adsorption rate strongly depends on the initial MB concentrations. The high adsorption of MB on amorphous WO_3 is associated with the combined effects of a large surface area and strong electrostatic interaction between cationic MB molecules and negative surface charge of WO_3 SMRs. The high adsorption capability along with the capability to break down toxic dyes into safe by-products, i.e. through the photocatalytic action under UV-irradiation, makes these WO_3 nanostructures promising candidates in the quest to remediate industrial pollution. However, for practical applications, besides the need of large quantity of the WO_3 SMRs, other environmental factors such as inorganic electrolytes and dissolved metal ions could affect the adsorption capability of WO_3, and need to be studied extensively.

Acknowledgements

This project was supported by an Agriculture and Food Research Initiative Grant no. 2011-68003-30012 from the USDA National Institute of Food and Agriculture, Food Safety: Food Processing Technologies to Destroy Food-borne Pathogens Program - (A4131). The authors would like to thank Mr. Taku Cowger for taking the TEM images and Mr. George Larsen for proofreading the manuscript.

Supporting Information

Detailed description of WO_3 SMRs sample preparation method, including structural and optical characterizations. Details of the MB adsorption experiment. FT-IR and optical absorption spectra of MB adsorbed WO_3 SMRs. Comparison of MB concentration change behaviors under dark adsorption and photocatalytic decay. Calibration curve and concentrations of MB aqueous solutions. SEM and TEM images of sponge-like nanoscale networks formed after the adsorption experiment with centrifugation**.** Comparisons of equilibrium adsorption capacities, q_e for amorphous and crystalline WO_3 SMRs. Comparisons of q_e for cationic and anionic dyes. Pseudo-first-order kinetic model and result comparisons with pseudo-second-order model.

See DOI:

Notes and references

1. F.-C. Wu and R.-L. Tseng, *Journal of Hazardous Materials*, 2008, **152**, 1256-1267.
2. I. K. Konstantinou and T. A. Albanis, *Applied Catalysis B-Environmental*, 2004, **49**, 1-14.
3. G. Crini, *Bioresource Technology*, 2006, **97**, 1061-1085.
4. M. Rafatullah, O. Sulaiman, R. Hashim and A. Ahmad, *Journal of Hazardous Materials*, 2010, **177**, 70-80.
5. V. K. Garg, M. Amita, R. Kumar and R. Gupta, *Dyes and Pigments*, 2004, **63**, 243-250.
6. N. Kannan and M. M. Sundaram, *Dyes and Pigments*, 2001, **51**, 25-40.
7. C. D. Woolard, J. Strong and C. R. Erasmus, *Applied Geochemistry*, 2002, **17**, 1159-1164.

8. G. McKay, G. Ramprasad and P. P. Mowli, *Water Air and Soil Pollution*, 1986, **29**, 273-283.
9. M. T. Uddin, M. A. Islam, S. Mahmud and M. Rukanuzzaman, *Journal of Hazardous Materials*, 2009, **164**, 53-60.
10. T. Robinson, G. McMullan, R. Marchant and P. Nigam, *Bioresource Technology*, 2001, **77**, 247-255.
11. I. A. W. Tan, A. L. Ahmad and B. H. Hameed, *Journal of Hazardous Materials*, 2008, **154**, 337-346.
12. X. Zhuang, Y. Wan, C. Feng, Y. Shen and D. Zhao, *Chem Mater*, 2009, **21**, 706-716.
13. A. Gürses, Ç. Doğar, S. Karaca, M. Açikyildiz and R. Bayrak, *Journal of Hazardous Materials*, 2006, **131**, 254-259.
14. M. K. Purkait, A. Maiti, S. DasGupta and S. De, *Journal of Hazardous Materials*, 2007, **145**, 287-295.
15. W. Morales, M. Cason, O. Aina, N. R. de Tacconi and K. Rajeshwar, *Journal of the American Chemical Society*, 2008, **130**, 6318-6319.
16. L. Li, M. Krissanasaeranee, S. W. Pattinson, M. Stefik, U. Wiesner, U. Steiner and D. Eder, *Chemical Communications*, 2010, **46**, 7620-7622.
17. R. Zhu, S. Cong, Y. Tian, H. Li, M. Chen, Y. Huang, Z. Zhao and Q. Li, *Chemical Communications*, 2013, **49**, 5787-5789.
18. M. M. Hawkeye and M. J. Brett, *Journal of Vacuum Science & Technology A*, 2007, **25**, 1317-1335.
19. Y. He and Y. Zhao, *Nanoscale*, 2011, **3**, 2361-2375.
20. J. J. Steele and M. J. Brett, *J Mater Sci-Mater El*, 2007, **18**, 367-379.
21. S. Wang, G. Xia, H. He, K. Yi, J. Shao and Z. Fan, *J Alloy Compd*, 2007, **431**, 287-291.
22. I. Langmuir, *Journal of the American Chemical Society*, 1916, **38**, 2221-2295.
23. Y. S. Ho and G. McKay, *Process Biochemistry*, 1999, **34**, 451-465.
24. B. H. Hameed, A. L. Ahmad and K. N. A. Latiff, *Dyes and Pigments*, 2007, **75**, 143-149.
25. F. Wang, C. H. Li and J. C. Yu, *Sep Purif Technol*, 2012, **91**, 103-107.
26. J. A. Zhu, S. L. Wang, S. H. Xie and H. X. Li, *Chemical Communications*, 2011, **47**, 4403-4405.
27. S. Azizian, *J Colloid Interf Sci*, 2004, **276**, 47-52.
28. M. Doğan, Y. Özdemir and M. Alkan, *Dyes and Pigments*, 2007, **75**, 701-713.
29. W. T. Tsai, C. Y. Chang, C. H. Ing and C. F. Chang, *J Colloid Interf Sci*, 2004, **275**, 72-78.

Table 1 Summary of equilibrium adsorption capacities (q_e) of WO_3 related adsorbents, including experimental parameters

Adsorbent/ Phase	Dye/ C_0 (μM)	m/V (mg/mL)	q_e (mg/g)	Ref.
WO_3 particles / Monoclinic	MB/ 50.0	500/250	~ 8	Morales *et. al.*[15]
WO_3 NRs[¤]/ Hexagonal	MB/ 187.0	70/50	10 to 73	Zhu *et. al.*[26]
WO_3 NRs[¤]/ Hexagonal	MB/ 312.6	10/10	88	Wang *et. al.*[25]
Commercial AC[$] /(N/A)	MB/ 312.6	10/10	85.9	Wang *et. al.*[25]
WO_3 SMRs/Amorphous	MB/ 50.0	0.48/3.0	149.8	Our work
WO_3 SMRs /Amorphous	R6G/ 50.0	0.48/3.0	176.5	Our work
WO_3 SMRs / Monoclinic	MB/ 50.0	0.48/3.0	29.5	Our work
WO_3 SMRs / Mixed[#]	MB/ 50.0	0.48/3.0	22.8	Our work

NRs[¤] (nanorods) AC[$] (activated carbon), and [#]Mixed = Monoclinic + Orthorhombic + Hexagonal (mixed phase)

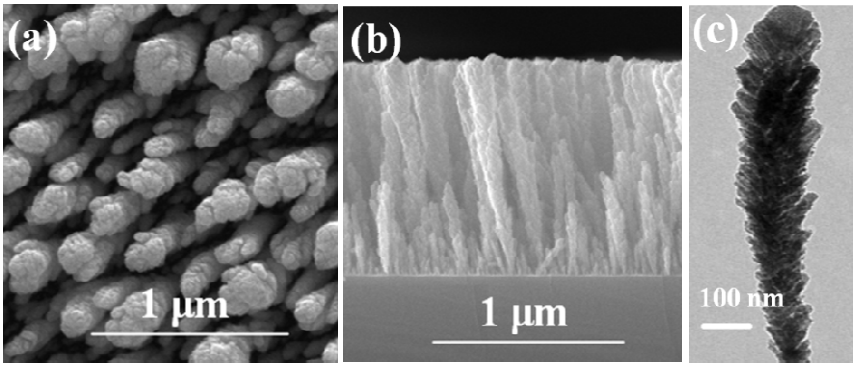

Fig. 1 (a) Top-view and (b) cross-section SEM micrographs of as-deposited WO_3 GLAD SMRs arrays. (c) A TEM image showing the highly porous morphology of WO_3 SMRs.

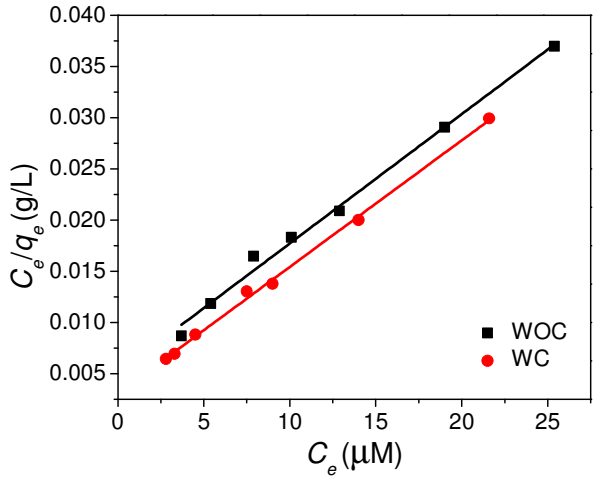

Fig. 2 Langmuir plot of adsorption isotherms.

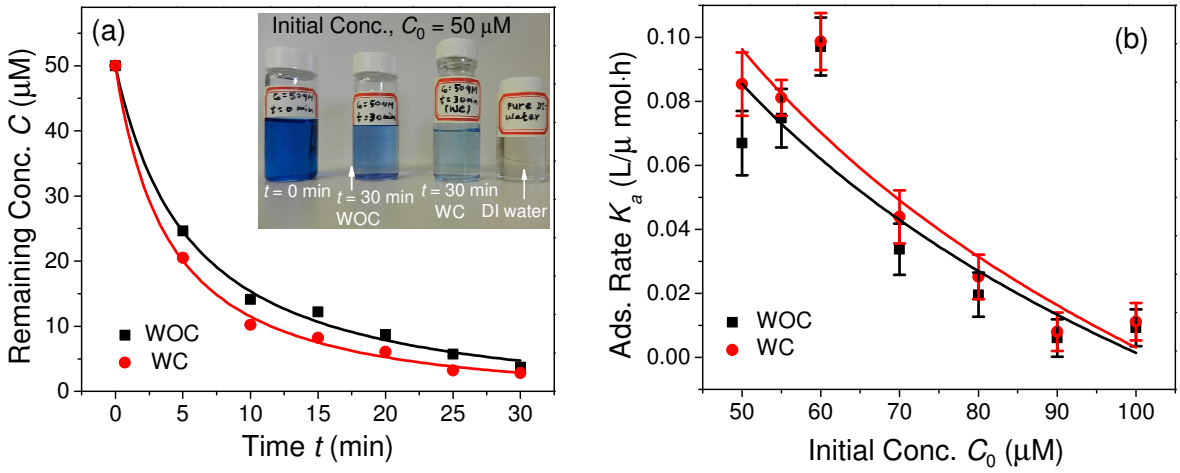

Fig. 3 (a) Time dependent MB concentration C (t) for C_0 = 50 μM for WOC and WC processes. The inset shows the decoloration of MB solution before and after equilibrium adsorption. (b) Adsorption constants K_a *versus* the MB concentration C_0 for WOC and WC cases. Symbols represent experimental data and the solid curves are a guide to eye. Error bars in Fig. 3b represent the estimated errors in data fittings.